

# First Simultaneous NIR/X-ray Detection of a Flare from SgrA\*

A. Eckart<sup>1</sup>, F. K. Baganoff<sup>2</sup>, M. Morris<sup>3</sup>, M.W. Bautz<sup>2</sup>, W.N. Brandt<sup>4</sup>, G.P. Garmire<sup>4</sup>,  
R. Genzel<sup>5</sup>, T. Ott<sup>5</sup>, G.R. Ricker<sup>4</sup>, C. Straubmeier<sup>1</sup>, T. Viehmann<sup>1</sup>, and R. Schödel<sup>1</sup>

<sup>1</sup> I.Physikalisches Institut, Universität zu Köln, Zülpicher Str.77, 50937 Köln  
e-mail: eckart@ph1.uni-koeln.de

<sup>2</sup> Center for Space Research, Massachusetts Institute of Technology, Cambridge, MA  
02139-4307, USA  
e-mail: fkb@space.mit.edu

<sup>3</sup> University of California Los Angeles, USA

<sup>4</sup> Department of Astronomy and Astrophysics, Pennsylvania State University, University  
Park, PA, 16802-6305 USA

<sup>5</sup> Max Planck Institut für extraterrestrische Physik, Giessenbachstraße, 85748 Garching,  
Germany

Received ; Accepted

**Abstract.** We report on the first simultaneous near-infrared/X-ray detection of the SgrA\* counterpart which is associated with the massive  $3-4 \times 10^6 M_\odot$  black hole at the center of the Milky Way. The observations have been carried out using the NACO adaptive optics (AO) instrument at the European Southern Observatory's Very Large Telescope\* and the ACIS-I instrument aboard the *Chandra X-ray observatory*. A flare was detected in the X-ray domain with an excess 2 - 10 keV luminosity of about  $6 \times 10^{33}$  erg/s. The NIR observations began near the peak of the X-ray flare and detected a fading NIR flare of Sgr A\* with  $> 2$  times the interim-quiescent flux. We find that the flaring state can be conveniently explained with a synchrotron self-Compton model involving up-scattered sub-millimeter photons from a compact source component showing bulk relativistic motion. The size of that component is assumed to be of the order of the Schwarzschild radius. The overall spectral indices  $\alpha_{NIR/X-ray}$  ( $S_\nu \propto \nu^{-\alpha}$ ) of both states are consistent with a value of  $\sim 1.3$ . Since the interim-quiescent X-ray emission is extended, the spectral index for the interim-quiescent state is only a lower limit for the compact source Sgr A\*. A conservative estimate of the upper limit of the time lag between the end of the NIR and X-ray flare is of the order of 15 minutes.

\* Based on observations at the Very Large Telescope (VLT) of the European Southern Observatory (ESO) on Paranal in Chile; Program: 271.B-5019(A).

**Key words.** Sagittarius A\* – Black Hole – Galactic Center – Flare – X-ray – Near Infrared

## 1. Introduction

Over the last few decades, evidence has been accumulating that most quiet galaxies harbor massive black holes (MBHs) at their centers. Especially in the case of the center of our Galaxy, progress could be made through the investigation of the dynamics of stars (Eckart & Genzel 1996, Genzel et al. 1997, 2000, Ghez et al. 1998, 2000, 2003a, 2003b, Eckart et al. 2002, Schödel et al. 2002, 2003). Located at a distance of only 8 kpc from the solar system (Reid 1993, Eisenhauer et al. 2003), it allows detailed observations of stars at distances much less than 1 pc from the central black hole candidate, the radio source Sgr A\*. Additional strong evidence for a massive black hole at the position of the compact radio source Sgr A\* came from the observation of interim-quiescent and flare activity from that position both in the X-ray and recently in the near-infrared wavelength domains (Baganoff et al. 2001, 2003a, Eckart et al. 2003, Porquet et al. 2003, Goldwurm et al. 2003, Ghez et al. 2004, Genzel et al. 2003). Throughout the paper we will use the term 'interim-quiescent' (or IQ) for the apparently constant, low-level flux density states at any given observational epoch since current data cannot exclude flux density variations of that state on longer time scales (days to years). This is especially true for the better resolved NIR source (Genzel et al. 2003, Ghez et al. 2004).

Simultaneous observations of SgrA\* across different wavelength regimes are of high value, since they provide information on the emission mechanisms responsible for the radiation from the immediate vicinity of the central black hole. The first observations of SgrA\* covering an X-ray flare simultaneously in the near-infrared using seeing limited exposures revealed only upper limits to the NIR flux density (Eckart et al. 2003). In section 2 of the present paper we report on the first successful simultaneous NIR/X-ray observations using adaptive optics. A detailed statistical analysis that supports the simultaneous detection of a SgrA\* flare event in the NIR and X-ray domains is given in section 3 of this paper. In section 4 we briefly discuss the flux densities and spectral indices we derived from the available data. Section 5 gives a first physical interpretation of the simultaneous detection of SgrA\*. A short summary and discussion of the results is given in section 6.

## 2. Observations and Data Reduction

The Galactic Center stellar cluster was observed during Directors Discretionary Time on June 19, 2003, with the NAOS/CONICA adaptive optics system/NIR camera at the ESO VLT unit telescope 4. The loop of the AO was closed on the bright ( $K \sim 6.5$ ) supergiant IRS 7, located about 6" north of Sgr A\*. We used the  $K_S$ -filter ( $\lambda_C = 2.18\mu\text{m}$ , FWHM  $0.35\mu\text{m}$ ). The detector integration time was 10 s, with two frames added online to final exposures of 20 s integration time. The visible seeing at zenith was around 0.8". The AO correction was stable, but of medium quality

with an estimated Strehl ratio above 20% most of the time. The correction improved during the course of the observations, coincident with the decreasing airmass.

The individual exposures were sky subtracted, flat-fielded and corrected for bad pixels. We extracted PSFs for each of the images with *StarFinder* and used the extracted PSFs for a Lucy-Richardson deconvolution of all the images. After beam restoration with a Gaussian PSF of 60 mas FWHM, we extracted the fluxes of individual sources with aperture photometry. The stars W6,  $m_K=14.3\pm0.2$ , W9,  $m_K=13.7\pm0.2$ , and W11,  $m_K=14.1\pm0.2$ , (Ott 2003) were contained in all the images and were used for the photometric calibration. We repeated the photometric measurements with two different aperture sizes (26 and 39 mas) and took the average of these measurements as the source fluxes, with the errors given by the maximum deviation of the individual measurements from the average. We chose these small aperture sizes in order to minimize contamination of the measured fluxes by close-by sources, a difficulty that arises especially near the location of Sgr A\*, where the stellar cusp peaks (Genzel et al. 2003). We derived extinction corrected fluxes, assuming  $A_K = 2.8$  (Genzel et al. 2003).

In the top panel of Figure 1 we show the light curves of Sgr A\*, and of the two stars S1 and S2 (top curves: fluxes of S1 and S2 are multiplied by a factor of 1.2), that are located in its immediate vicinity. In order to estimate the background, we averaged aperture photometric measurements from six random locations within a region with no detectable source, about 0.5'' W of SgrA\* (Figure 1, bottom light curve). For a better visualization of the flux variations of Sgr A\* during the first 60 min, the middle panel of Figure 1 shows the light curves of the upper panel after smoothing them with a sliding window that averages four measurements at a time. As can be seen in the middle panel of Figure 1, there appears still to be some correlated remnant flux variations. Therefore, we used three sources for an additional calibration (S1, S2, and S8, all within 0.5'' of Sgr A\*) that have been constant in previous observations and could largely remove these variations. The resulting light curves are shown in the lower panel of Figure 1.

The gaps in the measurements are due to AO reconfiguration or sky measurements. AO correction was poor during the first ten minutes of the observations. Four of the first twelve exposures had to be discarded from the data set. The low AO performance at the beginning of the observations is the reason for the larger error bars and the increased background level at the beginning of the light curves. In comparison to the light curves of the background, S1, and S2 (that are assumed to have a constant flux, of course), the flux of Sgr A\* is clearly higher ( $> 5\sigma$  as can be seen in the lower, averaged plot) at the beginning of the observations and decreases until it reaches almost the background level. Apparently, there remains some substructure in the flux variation of Sgr A\*. But while the small flux increases around 85 min and 135 min appear to be significant, we believe that the sub-structure (the “bump”) at the very beginning of the light curve is questionable because of the poorer quality of the data at the very beginning of the observations. However, the overall flux is significantly higher at the beginning of the observations.

Because of faint stellar sources very close to the position of Sgr A\*, that can be detected when one averages the individual images, we estimate a possible systematic positive bias of the flux of Sgr A\*, of the order of 0.5 to 1.0 mJy.

The flaring of Sgr A\* can be seen in Figure 2. In the top panel we show the average of eight images at the beginning of the observations. The middle panel shows the average of eight images that were obtained about 25 min after the beginning of the observations. Eight images about 80 min into the observations are averaged in the bottom panel. The UTs of the first image of each series are indicated in all the panels. All images resulted after Lucy-Richardson deconvolution and beam restoration. One can see how the AO correction improved between images 1 and 2. Sgr A\* can be seen as a flaring source in the first two images and is not visible in the last image.

The offset of the flaring source from the dynamical position of SgrA\* - taking into account the orbit of S2 (Schödel et al. 2003) - is  $6 \pm 2$  mas in R.A. and  $12 \pm 4$  mas in Dec. and well within the values obtained for the previously detected flares of SgrA\* (Ghez et al. 2004, Genzel et al. 2003). The deviation from the nominal position of Sgr A\* is most probably due to the weakness of the flare and to the proximity of faint stellar sources.

In parallel to the NIR observations SgrA\* was observed with *Chandra* using the imaging array of the Advanced CCD Imaging Spectrometer (ACIS-I; Weisskopf et al. 2002) for 25,115.48 s on 19–20 June 2003 (UT). The start and stop times are listed in Table 1. The instrument was operated in timed exposure mode with detectors I0–3 turned on. The time between CCD frames was 3.14104 s. The event data were telemetered in faint format.

We reduced and analyzed the data using the CIAO v2.3<sup>1</sup> software with Chandra CALDB v2.22<sup>2</sup>. Following Baganoff et al. (2003), we reprocessed the level 1 data to remove the 0.25'' randomization of event positions applied during standard pipeline processing and to retain events flagged as possible cosmic-ray afterglows, since the strong diffuse emission in the Galactic Center causes the algorithm to flag a significant fraction of genuine X-rays. The data were filtered on the standard ASCA grades. The background was stable throughout the observation, and there were no gaps in the telemetry.

The X-ray and optical positions of three Tycho-2 sources were correlated (Høg 2000) to register the ACIS field on the Hipparcos coordinate frame to an accuracy of 0.10'' (on axis); then we measured the position of the X-ray source at Sgr A\*. The X-ray position [R.A. =  $17^{\text{h}}45^{\text{m}}40.030^{\text{s}}$ , decl. =  $-29^{\circ}00'28.23''$  (J2000.0)] is consistent with the radio position of Sgr A\* (Reid et al., 1999) to within  $0.18'' \pm 0.18''$  ( $1\sigma$ ).

We extracted counts within radii of 0.5'', 1.0'', and 1.5'' around Sgr A\* in the 2–8 keV band. Background counts were extracted from an annulus around Sgr A\* with inner and outer radii of 2'' and 10'', respectively, excluding regions around discrete sources and bright structures (see Baganoff et al. 2003). The mean count rates within each radius are listed in Table 2. The background rates have been scaled to the area of the source region. We note that the mean source rate

<sup>1</sup> Chandra Interactive Analysis of Observations (CIAO), <http://cxc.harvard.edu/ciao>

<sup>2</sup> <http://cxc.harvard.edu/caldb>

in the  $1.5''$  aperture is consistent with the mean quiescent source rates from previous observations (Baganoff et al. 2001, 2003). The PSF encircled energy within each aperture increases from  $\approx 50\%$  for the smallest radius to  $\approx 90\%$  for the largest, while the estimated fraction of counts from background increases with radius from  $\approx 5\%$  to  $\approx 11\%$ . Thus, the  $1.0''$  aperture provides the best compromise between maximizing source signal and rejecting background.

### 3. Variability Analysis

Figures 1 and 2 show the clear detection of a decaying flare in the NIR emission of SgrA\*. This flare is accompanied by an apparently simultaneous flare event in the X-ray domain (see Figures 3 and 4). The following analysis consolidates the significance of the X-ray flare and the correlation with the NIR flare event.

As a first step in our variability analysis, we constructed binned light curves of the X-ray source intensity for each aperture using 10 minute bins, and then we tested each curve against the null hypothesis of a constant count rate. The  $\chi^2$  statistic and degrees of freedom for each fit are listed in Table 2. In each case, a constant count rate yielded an acceptable fit to the data; for such low count rates, however,  $\chi^2$  analyses of binned light curves are not particularly sensitive tests for variability.

Figure 3 shows the source and background light curves for the  $1.0''$  aperture. We note that the three highest points are clustered within a 40 minute interval centered around 300 minutes after the start of the *Chandra* observation. The first VLT/NACO image was taken about 305 min after the start of the X-ray observations. The NIR light curve in Figure 2 shows clearly that Sgr A\* was in a flaring state at this time.

To investigate this further, we applied a standard Kolmogorov-Smirnov (K-S) test to the arrival times of the X-ray photons within each aperture. Multiple photons were occasionally detected in the same CCD frame. We corrected for this by redistributing their arrival times over the frame interval using uniform random deviates. The K-S test revealed no evidence for significant variability (see Table 3). The sensitivity of this test, however, depends on the location of the maximum deviation along the distribution. Press et al. (1992) present a variant of the K-S test called the Kuiper test (Kuiper 1962) that solves this problem by using the sum of the maximum deviations of the observed cumulative distribution *above* and *below* the theoretical distribution rather than the maximum absolute deviation used in the K-S test. The results of the Kuiper test are shown in Table 3. The evidence for variability in the  $1.0''$  and  $1.5''$  apertures, which contain a higher fraction of background counts from diffuse emission, was marginally significant:  $\approx 95\%$  confidence. The evidence for variability in the  $0.5''$  aperture was highly significant: 99.4% confidence. The results of the Kuiper test thus suggest that Sgr A\* varied in X-rays; even so, it gives us no objective information about the location, duration, and amplitude of the variability.

A flexible method for obtaining such information is the Bayesian blocks algorithm of Scargle (1998), which uses the Poisson distribution and Bayesian statistics to partition an interval of data

into piecewise constant segments or blocks. Each block is modeled as a Poisson process with constant intensity. The boundaries between adjacent blocks mark transitions from one Poisson rate to another, and are called change points. The final model represents the data as a set of change points, defining the start and stop times of each block, and a corresponding set of Poisson rates, one for each block. A revised version (Scargle et al. 2004) of the original method incorporates an algorithm for finding the *global, optimal* partitioning of data on an interval (Jackson et al., 2003).

The algorithm uses a geometric prior of the form  $P(k) = C\gamma^{-k}$ , where  $k$  is the number of change points,  $P(k)$  is the prior probability distribution on the number of change points, and  $\gamma$  is an adjustable parameter (Scargle et al., 2003, 2004). Taking the logarithm of both sides yields the following contribution to the log-posterior:  $\log P(k) = \log C - k \log \gamma$ . This additive term in the fitness function penalizes more complex models; that is, models with more blocks. Setting  $\gamma = 1$  corresponds to choosing a uniform prior,  $P(k) = C$ , where all values of  $k$  are equally likely. The higher  $\gamma$  is set, the harder it becomes for the algorithm to add change points defining more blocks.

The value of  $\gamma$  can be converted into a prior odds ratio,  $P(k \geq 1)/P(0)$ , giving the ratio—before analyzing the data—of the probability that the source varied at all to the probability that it was constant. This would equal  $1/(\gamma-1)$  for an infinite geometric series, but  $k$  can never be greater than the number of detected photons, so the actual form of the odds ratio is more complicated (J. D. Scargle 2003, private communication). In practice, however, the series converges rapidly for  $\gamma \gg 1$ .

In Bayesian statistics, the posterior probability that the model is correct given the data is proportional to the product of the prior probability, expressing our knowledge or ignorance of the truth of the model before analyzing the data, and the likelihood function, which is the probability of the data given the model (Sivia 1996). As noted above, the prior odds ratio introduces a bias against more complex models. The preference of the data for the more complex model must be compelling enough to overcome the prior bias before the algorithm will introduce a new change point. In other words, the ratio of the likelihood functions for the data given the models must be greater than the inverse of the prior odds ratio.

We applied the global Bayesian blocks algorithm to a binned light curve of the total counts in the 1.0'' aperture using 157.052 second bins (i.e., 50 times the interval between CCD frames). Figure 5 shows the Bayesian blocks decomposition of the light curve obtained with  $\log \gamma = 3.35$ , corresponding to a prior odds ratio of  $4.47 \times 10^{-4}$ . Two change points were found at 279.1 and 321.2 minutes into the observation indicating that Sgr A\* flared in X-rays around midnight. Similar results were obtained for bin sizes ranging from 10 to 200 times the interval between CCD frames. No change points were found for values of  $\log \gamma > 3.35$ .

The mean count rates and start and stop times for the three blocks are presented in Table 4. The count rates during blocks 1 and 3 were consistent with each other. The mean rate for these

two intervals combined was  $(3.95 \pm 0.42) \times 10^{-3}$  counts s $^{-1}$ , whereas the mean rate during block 2 was  $(11.63 \pm 2.59) \times 10^{-3}$  counts s $^{-1}$ : a difference of  $(7.68 \pm 2.20) \times 10^{-3}$  counts s $^{-1}$ .

We performed Monte Carlo simulations to determine the posterior probability of obtaining a block with a rate greater than or equal to that of block 2. Using the mean rate over the entire observation (i.e.,  $4.40 \times 10^{-3}$  counts s $^{-1}$ ), we generated 100,000 simulated Poisson data sets with each set having the same number of counts as the real data. We then binned the counts into light curves and ran the Bayesian blocks algorithm on each simulated light curve as before. The algorithm gave a false positive rate or posterior probability of  $7.7 \times 10^{-4}$ , which is less than twice the prior odds ratio estimated above. Thus, the null hypothesis of a constant rate is rejected with 99.923% confidence, and we conclude that Sgr A\* flared in X-rays for a period of about 42 minutes, which is characteristic of both the X-ray and NIR flares detected in previous observations (Baganoff et al., 2001, 2003; Goldwurm et al., 2003; Porquet et al., 2003; Genzel et al., 2003; Ghez et al., 2004).

### 3.1. Properties of the Lightcurves

From linear fits to the data in the rising and decaying flanks of the X-ray and NIR flare including the measurement uncertainties (Figures 1 and 3) we can estimate the times at which the flare emission was negligible, i.e. equal to the IQ-state emission. The corresponding full width zero power (FWZP) and start and stop times (see Table 5) compare well with the times of the change points and widths derived from the Bayesian blocks routine. They are earlier and later than the respective turn-on and turn-off change points. Also an estimate of the FWHM (Table 5) of the flare from Figure 3 is comparable to the flare duration derived from the Bayesian blocks analysis.

Further support for the detection of a simultaneous flare at NIR and X-ray wavelengths comes from a cross-correlation between the variability data obtained in both domains. The analysis was performed on the measured NIR lightcurve (Figure 1, upper panel) and on the X-ray data shown in Figure 3. A constant flux density contribution of SgrA\* (see next section and Tab.1) was subtracted before the analysis. The cross-correlation was performed by shifting the entire NIR data set over a range of -30 to +50 minutes with respect to its beginning at 19 June 23:51:15 UT. We cross-correlated only the data that overlap in time. The result is shown in Figure 6. With respect to the noise for shifts of less than -20 and more than +20 minutes the cross-correlation shows a  $>5\sigma$  peak. The graph shows a clear maximum close to 0 minutes offset indicating that within the binning sizes both data sets are well correlated. A possible time lag between the X-ray and NIR data of about 10 minutes (with the X-ray data leading) is indicated. However, considering the bin sizes used, 10 minutes and 40 seconds, we regard  $\sim 15$  minutes as a conservative upper limit of any time lag between the NIR and X-ray emission that may have been present on the *decaying* flanks of the observed flare (Table 5).

In summary the statistical analysis of the combined X-ray and NIR data shows that SgrA\* underwent a significant flare event simultaneously in both wavelength regimes.

#### 4. Flux Densities and Spectral Indices

The IQ-state X-ray count rate in a 1.5" radius aperture of  $5.3 \pm 0.5 \times 10^{-3}$  counts s<sup>-1</sup> during the monitoring period is consistent with the rates measured during previous *Chandra* observations (Baganoff et al. 2001, 2003). It corresponds to a 2 - 10 keV luminosity of  $2.2 \times 10^{33}$  erg/s or a flux density of  $0.015 \mu\text{Jy}$ . The excess flux density observed during the simultaneous flare event was  $0.039 \mu\text{Jy}$ . In total flux density this is a factor of 3.6 higher and in excess flux density this is a factor of 2.6 higher than the IQ-state. This corresponds to a 2 - 10 keV luminosity of about  $6 \times 10^{33}$  erg/s. In the infrared the  $2.2\mu\text{m}$  flux density of the IQ-state Sgr A\* counterpart is 1.9 mJy and the excess flux density observed during the flare is 3.7 mJy (measured for the high S/N data points about 25 min after the beginning of the observations). Since we may have passed the peak of the NIR flare emission (see the previous section and compare Figures 1 and 3) this is in total flux density at least a factor of 2.9 higher and in excess flux density this is at least a factor of 1.9 higher than the IQ-state.

Hence, the spectral indices between the NIR regime (here at a wavelength of  $2.2\mu\text{m}$ ) and the X-ray domain (here centered approximately at an energy of 4 keV) of both the IQ- and the flaring states are very similar, with  $\alpha_{X/NIR} \sim 1.3$ .

For the IQ-state this spectral index is almost identical to  $\alpha_{X/NIR} \leq 1.36$  as calculated using the published flux density values in Baganoff et al. (2001, 2003a) and Genzel et al. (2003). However, with current data, it appears that the magnitude of the fluctuations is substantially larger at X-ray (Baganoff et al. 2001, 2003a; Porquet et al. 2003; Goldwurm et al. 2003) than at IR wavelengths (Genzel et al. 2003, Ghez et al. 2004), so that the spectral index could be smaller than about  $\alpha_{X/NIR} \leq 1.0$  if we simply take the most extreme fluxes so far measured at both wavelengths.

Our data also allow us to derive an estimate of the flux density rise- and decay-rates (Tab.1). These rates are essential quantities that describe possible combinations between time variations in the source geometry and the relevant energy release or dissipation processes. The fractional rate of decay is about 1–3%/min for both the X-ray and NIR regimes.

#### 5. Physical Interpretation

Current models that explain the SgrA\* spectral energy distribution invoke radiatively inefficient accretion flow models (RIAFs: Quataert 2003, Yuan et al. 2002, Yuan, Quataert, & Narayan 2003, 2004), including advection dominated accretion flows (ADAF): Narayan et al. 1995, convection dominated accretion flows (CDAF): Ball et al. 2001, Quataert & Gruzinov 2000, Narayan et al. 2002, Igumenshchev 2002, advection-dominated inflow-outflow solution (ADIOS): Blandford & Begelman 1999), jet models (Markoff et al. 2001), and Bondi-Hoyle models (Melia & Falke 2001).

Micro-lensing as a cause for the NIR variability can most likely be excluded because of the short duration of the events, their high frequency of occurrence, and the shape of their light curves (see also Porquet et al., 2003; Ghez et al., 2004; and Genzel et al., 2003). The model in

which stars interact with an inactive, cold accretion disk (Nayakshin, Cuadra & Sunyaev 2004, Nayakshin & Sunyaev 2003) is also not a very satisfactory explanation for the NIR flares. To within a few milliarcseconds the emission peaks of all NIR flares observed so far (Genzel et al. 2003, Ghez et al. 2004) are located at the position of the radio source SgrA\*. However, the most likely inner disk radius required by the cold disk model is of the order of 10mas (Nayakshin & Sunyaev 2003), implying that all the flares did not occur within such a disk. In addition, this model does not provide an explanation for the  $\sim$ 17 minute quasi-periodic fine structure observed in 2 of the flares (Genzel et al. 2003). An analysis of the two brightest X-ray flares also shows a temporal power spectrum that is incompatible with the cold disk model (Aschenbach et al., 2004).

For the IQ-phase the theoretical models have to take into account that the X-ray flux density is extended over the central 0.6 arcsecond radius, while the flaring source is a point source (Baganoff et al., 2001, 2003a). For the flare activity the short variation time scale presents an additional complication to these models. Thermal bremsstrahlung emission from the outer regions of an accretion flow ( $R > 10^3 R_s$ ; see also Quataert 2003) would not be able to explain the observed rapid variations of the X-ray flux density. Flare models involving bremsstrahlung would require multiple components of plasma at different temperatures because the NIR emission requires a component of significantly lower temperature than the X-ray emission (Genzel et al. 2003). Pure synchrotron emission models require a high energy cutoff in the electron energy distribution with large Lorentz factors for the emitting electrons of  $\gamma_e > 10^5$  and magnetic field strengths of the order of 10-100 G in order to explain the X-ray emission. The correspondingly short cooling time scales of less than a few hundred seconds would then require either repeated injections or repeated heating/acceleration of such energetic particles (Baganoff et al 2001; Markoff et al. 2001; Yuan, Quataert, & Narayan 2004).

Our new simultaneous X-ray/NIR detection of the SgrA\* counterpart suggests that at least for the observed flare it is the same population of electrons that is responsible for both the IR and the X-ray emission, regardless of the emission mechanism. While it is not yet possible to completely rule out any of the proposed models, we find that an attractive mechanism to explain the observed simultaneous NIR/X-ray flare is the synchrotron self-Compton (SSC) process. In this model, the X-ray photons are produced by up-scattering of sub-millimeter photons. The SSC process directly couples both the NIR and X-ray emission to the sub-mm-domain and would naturally result in low upper limits on any measurable time lag between the NIR and X-ray emission (see Table 5 and section 4). The short time scale of the observed flux density variations indicates that the flare emission originates from compact components within  $\sim$ 10 Schwarzschild radii  $R_s = 2GM/c^2$  with  $R_s = 8.8 \times 10^9$  m for a  $3 \times 10^6 M_\odot$  black hole. At a distance to the Galactic Center of 8 kpc (Reid 1993, Eisenhauer et al. 2003) this corresponds to an angular diameter of  $6.8 \times 10^{-3}$  mas. For such a component the inverse Compton scattered flux density will depend on the relativistic bulk motion of the emitting source with a Doppler boosting factor  $\delta = \Gamma^{-1}(1 - \beta \cos \phi)^{-1}$ . Here  $\phi$  is the angle of the velocity vector to the line of sight,  $\beta$  the ve-

locity  $v$  in units of the speed of light  $c$ , and  $\Gamma = (1 - \beta^2)^{-1/2}$  is the Lorentz factor for the bulk motion.

Doppler boosting will occur in models that involve relativistic jets pointing toward the observer at a small angle to the line of sight (e.g. Markoff et al. 2001). In the context of this jet model, the emitting component would be located close to the jet base and would have a size of a few  $R_s$  or less. It can also occur in a model in which matter is orbiting the black hole at small angles of the orbital plane with respect to the observer's line of sight and close to the innermost stable orbits (Bardeen, Press, & Teukolsky 1972; Melia et al. 2001). In this case the dominant component responsible for a flare would be the Doppler boosted material moving toward the observer. The component size could then be of the order of a fraction of the Schwarzschild radius  $R_s$ . In the following we assume that the dominant component responsible for a flare has a size that is of the order of  $R_s$ . In such a model the rising and fading times of the observed flares (Baganoff et al. 2001; Genzel et al. 2003) of a few tens of minutes (see Table 5) could therefore be explained quite conveniently by Doppler boosting. If the matter or temperature distribution or the spatial distribution of electrons in the high-energy tail of the electron energy distribution over these orbits deviates significantly from a homogenous distribution such a model would also be appropriate to explain the quasi-periodic flux density variations observed in two NIR flares (Genzel et al. 2003). In this model more homogenous distributions would also explain non-periodic variations over longer time scales, i.e. the overall flare shape, by Doppler boosting of the approaching side of the orbit.

We can compute the SSC spectrum produced by up-scattering sub-mm-wavelength photons into the NIR and X-ray domains by using the formalism given by Gould (1979) and Marscher (1983). Such a single SSC component model may be too simplistic but can be considered as a viable first approach. For the single-component SSC model discussed in this paper, our data suggest a NIR to X-ray spectral index of 1.3. This is inconsistent with the X-ray spectral index of 0.3 observed by Chandra, although it is consistent with the spectral index of  $1.5 \pm 0.3$  reported by Porquet et al. (2003). The spectral index, however, is a strong function of the assumed ISM abundances and the calculation presented here should be taken as an illustrative example for a simple physical scenario. We use the notation by Marscher et al. (1983) and assume a synchrotron source of angular extent  $\theta$ , that becomes optically thick at a frequency  $\nu_m$  with a flux density  $S_m$ , and has an optically thin spectral index  $\alpha$  following the law  $S_\nu \propto \nu^{-\alpha}$ . This allows us to calculate the magnetic field strength  $B$  and the inverse Compton scattered flux density  $S_{SSC}$  as a function of the X-ray photon energy  $E_{keV}$ . The synchrotron self-Compton spectrum has the same spectral index as the up-scattered synchrotron spectrum, i.e.  $S_{SSC} \propto E_{keV}^{-\alpha}$ , and is valid within the limits  $E_{min}$  and  $E_{max}$  corresponding to the wavelengths  $\lambda_{min}$  and  $\lambda_{max}$  (see Marscher et al. 1983 for further details).

We find that the flux densities  $S_{2.2\mu m}$  and  $S_{X-ray}$  of the observed simultaneous flare event can be explained very well for cases in which the sub-millimeter emitting source component has a size of the order of  $R_s$  (or just smaller than that) and a turnover frequency  $\nu_m$  around 300 GHz.

For a relativistic bulk motion of the emitting component with  $\Gamma=10^2\text{-}10^3$  and  $\delta$  ranging between 0.1 and a few (i.e. angles  $\phi$  between about  $1^\circ$  and  $10^\circ$ ) the corresponding magnetic field strengths are of the order of 0.2 to 20 Gauss and the SSC spectrum is defined over a contiguous wavelength range between the infrared to the X-ray domains. The low-frequency cutoff of that up-scattered SSC spectrum is at wavelengths between a few  $10\text{-}100\mu\text{m}$  and the high-energy cutoff reaches energies between 10 keV to a few 100 keV. The required mm-flux densities  $S_m$  are only of the order of a fraction of a Jansky and well within the range of observed variability of SgrA\* in the mm-domain (Zhao et al. 2003). This simple SSC model would result in no time lag between the NIR and X-ray emission - compatible with our limit on the time lag for the decaying flank of the flare.

## 6. Summary and Discussion

We have presented the first successful simultaneous X-ray and NIR detections of SgrA\* in a flaring and the IQ-state. The X-ray flare lasted for about 42 minutes and began on 19 June 2003 at about 23:10 UT, more than 4 hours into the X-ray observation. The peak of the flare occurred only 10–20 minutes prior to the time of the first VLT/NACO DDT image. The emission during the flare can successfully be described by a SSC model in which the NIR and X-ray flux density excesses are produced by up-scattering sub-mm-wavelength photons into the NIR and X-ray domains.

With respect to its FWZP duration of 55 - 115 minutes the flare reported here compares well with other flares measured so far. Baganoff et al. (2001), Eckart et al. (2003), and Porquet et al. (2003) report on X-ray events of 45 to 170 minutes. Ghez et al. (2004) and Genzel et al. (2003) report on NIR flare events that last 50 to 80 minutes, respectively. Our newly detected flare event is weaker than most others which have been reported and not necessarily representative of the characteristics of the stronger flares (factor of 50: Baganoff et al. 2001; factor of >100: Porquet et al. 2003; Goldwurm et al. 2003). However, during our 2002 *Chandra* monitoring session we found that flares that are a factor of >10 stronger than the quiescent emission occur at a rate of  $0.53 \pm 0.27$  per day (Baganoff et al. 2004, in preparation). Weaker flares are more frequent, and our newly detected flare event is probably more representative of those weaker flares.

Although we have given preference to a simple SSC model in explaining the observed simultaneous flare emission, flux density contributions via other emission mechanisms may be of relevance. Along with enhanced electron heating leading to SSC flares, Markoff et al. (2001) also suggested the possibility that the flares may result from acceleration. This could result from electrons which are energetic enough to account for both the NIR and X-ray flares via direct synchrotron radiation. In fact even the SSC models presented by Markoff et al. (2001) and Yuan, Quataert, & Narayan (2003) result in a significant amount of direct synchrotron emission in the infrared (see also synchrotron models in Yuan, Quataert, & Narayan 2004). The different possible emission mechanisms may also be coupled in a more complicated way. Ambient thermal

electrons may be heated during a flare and may produce excess sub-millimeter and infrared flux density. This process could lead to correlated radio/NIR/X-ray variability quite similar to what is expected in SSC models (Yuan, Quataert, & Narayan 2003, 2004, Genzel et al. 2003, Ghez et al. 2004). These synchrotron/ inverse Compton models may also result in small (or no) time lag between the NIR and X-ray emission - compatible with our limit on the time lag for the decaying flank of the flare. In such a scenario it will be difficult to determine the relative importance and flux density contributions of the different emission mechanisms by variability.

Since the X-ray source responsible for most of the X-ray IQ-state flux density of SgrA\* is extended over a radius of about 0.6 arcsec (Baganoff et al. 2003), its emission can most likely be ascribed to bremsstrahlung from a thermal particle distribution. While the interim-quiescent NIR flux density probably can be attributed to a fairly compact component (Genzel et al. 2003), it is currently not clear how much of the quiescent X-ray flux density originates from that compact region. The extended X-ray component probably originates from hot gas within the  $\sim 1''$  Bondi radius that is associated with the accretion flow (see Baganoff 2003 and Quataert 2003 for detailed discussions).

If thermal bremsstrahlung is an important mechanism to explain the simultaneous NIR and the X-ray emission, then geometries are conceivable in which the cooler  $\gtrsim 10^3$  K plasma that gives rise to the NIR emission is spatially offset from the hotter  $\gtrsim 10^8$  K plasma. One may also speculate that the amount of cooler plasma might be larger than the amount of hot plasma. These facts could result in a situation in which the X-ray variations lead the NIR-variations. On the other hand the cooling timescales of the hotter plasma may be larger which would result in the opposite behaviour. There are of course also models conceivable that involve small source sizes or apparently cospatial distributions that would result in no measurable time lag or even NIR and X-ray flare events that need not always be correlated (see discussion by Yuan, Quataert, & Narayan 2004).

Upcoming simultaneous monitoring programs from the radio to the X-ray regime will be required to further investigate the physical processes that give rise to the observed IQ-state and flare phenomena associated with SgrA\* at the position of the massive black hole at the center of the Milky Way.

*Acknowledgements.* This work was supported in part by the Deutsche Forschungsgemeinschaft (DFG) via grant SFB 494. *Chandra* research is supported by NASA grants NAS8-00128, NAS8-38252 and GO2-3115B. We are grateful to all members of the NAOS/ CONICA team. In particular we thank the ESO Director General C. Cesarsky for supporting this project via Directors Discretionary Time. We are also greatful to N. Ageorges and L. Tacconi-Garman for discussions and support.

We thank J. Scargle for his explanations of the Bayesian blocks method, and for his advice on numerical methods to determine the posterior probability of features of interest in the resultant segmented model. We also thank M. Nowak for coding the Bayesian blocks algorithm into S-Lang, and for discussing various aspects of the numerical implementation of the method.

## References

Aschenbach, B., Grosso, N., Porquet, D., & Predehl, P. 2004, A&A, in press (astro-ph/0401589)

Ball, G. H., Narayan, R. & Quataert, E. 2001, ApJ, 552, 221

Baganoff, F.K., Bautz, M.W., Brandt, W.N., et al. 2001, Nature, 413, 45

Baganoff, F. K., Maeda, Y., Morris, M., et al. 2003, ApJ 591, 891

Bardeen, J.M., Press, W.M., & Teukolsky, S.A. 1972, ApJ 178, 347

Blandford, R., & Begelman, M., 1999, MNRAS, 303, L1

Eckart, A. & Genzel, R. 1996, Nature 383, 415

Eckart, A., Genzel, R., Ott, T. and Schoedel, R. 2002, MNRAS, 331, 917

Eckart, A., Mouttaka, J., Viehmann, T. et al., 2003: Monitoring Sagittarius A\* in the MIR with the VLT. In: Proceedings of the Galactic Center Workshop, Nov. 3-8, 2002, Hawaii, A. Cotera, T. Geballe, S. Markoff, H. Falcke (editors), Astron. Nachr. 324, 2004

Eisenhauer, F., Schoedel, R., Genzel, R., et al. 2003, ApJ, 597, L121

Gehrels, N. 1986, ApJ, 303, 336

Genzel, T., Eckart, A., Ott, T. & Eisenhauer, MNRAS 1997, 291, 219

Genzel, R., Pichon, C., Eckart, A., Gerhard, O.E., Ott, T. 2000, MNRAS 317, 348

Genzel, R., Schoedel, R., Ott, T., et al. 2003, Nature, 425, 934

Ghez, A., Klein, B.L., Morris, M. & Becklin, E.E. 1998, ApJ, 509, 678

Ghez, A., Morris, M., Becklin, E.E., Tanner, A. & Kremenek, T. 2000, Nature 407, 349

Ghez, A. M., Duchéne, G., Matthews, K., et al. 2003a, ApJ, 586, L127

Ghez, A.M., Salim, S., Hornstein, S.D., et al. 2003b, ApJ, submitted, astro-ph/0306130

Ghez, A.M., Wright, S.A., Matthews, K., et al. 2004, ApJ 601, 159

Goldwurm, A., Brion, E., Goldoni, P. et al. 2003, ApJ, 584, 751

Gould, R.J., 1979, A&A 76, 306

Høg, E., Fabricius, C., Makarov, V.V. et al. 2000, A&A, 355, L27

Igumenshchev, I.V., 2002, ApJ 577, 31

Jackson, B., Scargle, J. D., Barnes, D., et al. 2003, IEEE Signal Proc. Let., submitted [math/0309285]

Kim, D.-W., Cameron, R.A., Drake, J.J. et al. 2004, ApJS, 150, 19

Kuiper, N.H. 1962, Proceedings of the Koninglijke Akademie van Wetenschappen, ser. A., 63, 38

Markoff, S., Falcke, H., Yuan, F. & Biermann, P.L. 2001, A&A, 379, L13

Marscher, A.P. 1983, ApJ, 264, 296

Melia, F., Bromley, C., Liu, S., & Walker, C.K. 2001, ApJ, 554, L37

Melia, F. & Falcke, H. 2001a, ARA&A 39, 309

Narayan, R., Yi, I., & Mahadevan, R. 1995, Nature, 374, 623

Narayan, R., Quataert, E., Igumenshchev, I.V., & Abramowicz, M.A. 2002, ApJ, 577, 295

Nayakshin, S., & Sunyaev, R. 2003, MNRAS 343, L15

Nayakshin, S., Cuadra, J., Sunyaev, R. 2004, A&A 413, 173

Ott, T., PhD thesis 2003, Ludwig-Maximilians-Universität, Munich, Germany

Porquet, D., Predehl, P., Aschenbach, et al. 2003, A&A 407, L17

Press, W. H., Teukolsky, S. A., Vetterling, W. T., & Flannery, B. P. 1992, Numerical Recipes in C: the Art of Scientific Computing (2d ed.; Cambridge: Cambridge University Press)

Quataert, E., & Gruzinov, A. 2000, ApJ 539, 809

Quataert, E., Astron. Nachr., Vol. 324, No. S1 (2003), Special Supplement "The central 300 parsecs of the Milky Way", Eds. A. Cotera, H. Falcke, T. R. Geballe, S. Markoff, in press, (astro-ph/0304099)

Quataert, E., submitted to ApJ Letters astro-ph/0310446

Reid, M. J., Readhead, A. C. S., Vermeulen, R. C., & Treuhaft, R. N. 1999, ApJ, 524, 816

Scargle, J. D. 1998, ApJ, 504, 405

Scargle, J., Jackson, B., & Norris, J. 2003, in PHYSTAT2003, Conference on Statistical Problems in Particle Physics, Astrophysics, and Cosmology, <http://www-conf.slac.stanford.edu/phystat2003/papers/TUHT003.pdf>

Scargle, J. D., Norris, J., Jackson, B., et al. 2004, in preparation, <http://trotsky.arc.nasa.gov/~jeffrey/global.pdf>

Schödel, R., Ott, T., Genzel, R. et al. 2002, Nature, 419, 694

Schoedel, R., Genzel, R., Ott, et al. 2003, ApJ, 596, 1015

Sivia, D. S. 1996, Data Analysis: A Bayesian Tutorial (Oxford: Oxford Univ. Press)

Weisskopf, M. C., Brinkman, B., Canizares, C., et al. 2002, PASP, 114, 1

Yuan, F., Markoff, S. & Falcke, H. 2002, A&A, 854, 854

Yuan, F., Quataert, E. & Narayan, R. 2003, ApJ, 598, 301

Yuan, F., Quataert, E. & Narayan, R. 2004, ApJ, submitted (astro-ph 0401429)

Zhao, J.-H., Young, K. H., Herrnstein, R. M., et al. 2003, ApJ 586, L29

Telescope	Instrument	Energy/ $\lambda$	UT Start Time	UT Stop Time
<i>Chandra</i>	ACIS-I	2-8 keV	19 JUN 2003 18:46:38	20 JUN 2003 01:45:13
VLT UT4	NACO	2.18 $\mu$ m	19 JUN 2003 23:51:15	20 JUN 2003 03:53:58

**Table 1.** Observation Log.**Table 2.** X-ray Count Rates

Extraction Radius ( $''$ )	Count Rates <sup>1</sup>			$\chi^2/\text{d.o.f.}^2$	
	Total ( $\times 10^{-3}$ cts s $^{-1}$ )	Source ( $\times 10^{-3}$ cts s $^{-1}$ )	Background ( $\times 10^{-3}$ cts s $^{-1}$ )		
	0.5	1.61 $\pm$ 0.26	1.53 $\pm$ 0.10	0.080 $\pm$ 0.004	7.4/41
1.0	4.72 $\pm$ 0.44	4.40 $\pm$ 0.13	0.320 $\pm$ 0.017	17.4/41	
1.5	7.02 $\pm$ 0.53	6.30 $\pm$ 0.15	0.719 $\pm$ 0.038	20.8/41	

<sup>1</sup> ACIS-I count rate in 2-8 keV band.<sup>2</sup> Fit of constant-rate model to source light curve using one-sided 1 $\sigma$  errors from Gehrels (1986).**Table 3.** Cumulative Distribution Tests for X-ray Variability

Extraction Radius ( $''$ )	Total Counts (cts)	K-S V Statistic	P(> V)	Kuiper D Statistic	P(> D)	Variable
0.5	40	0.1654	0.2036	0.3198	0.0055	Y
1.0	117	0.1170	0.0752	0.1592	0.0490	?
1.5	174	0.0838	0.1651	0.1348	0.0362	?

**Table 4.** Bayesian Blocks Representation of X-ray Light Curve

Block	UT Start Time	UT Stop Time	Duration (s)	Counts <sup>1</sup>	Count Rate <sup>2</sup>
				(cts)	( $\times 10^{-3}$ cts s $^{-1}$ )
1	19 JUN 2003 18:46:37.85	19 JUN 2003 23:25:41.50	16743.65	65	3.93 $\pm$ 0.55
2	19 JUN 2003 23:25:41.50	20 JUN 2003 00:07:48.84	2527.34	29	11.63 $\pm$ 2.59
3	20 JUN 2003 00:07:48.84	20 JUN 2003 01:45:13.33	5844.48	23	3.99 $\pm$ 1.02

<sup>1</sup> Total ACIS-I counts within 1.0'' radius of Sgr A\* in 2-8 keV band.<sup>2</sup> Corrected for dead time between CCD frames; the correction factor is 0.98693.

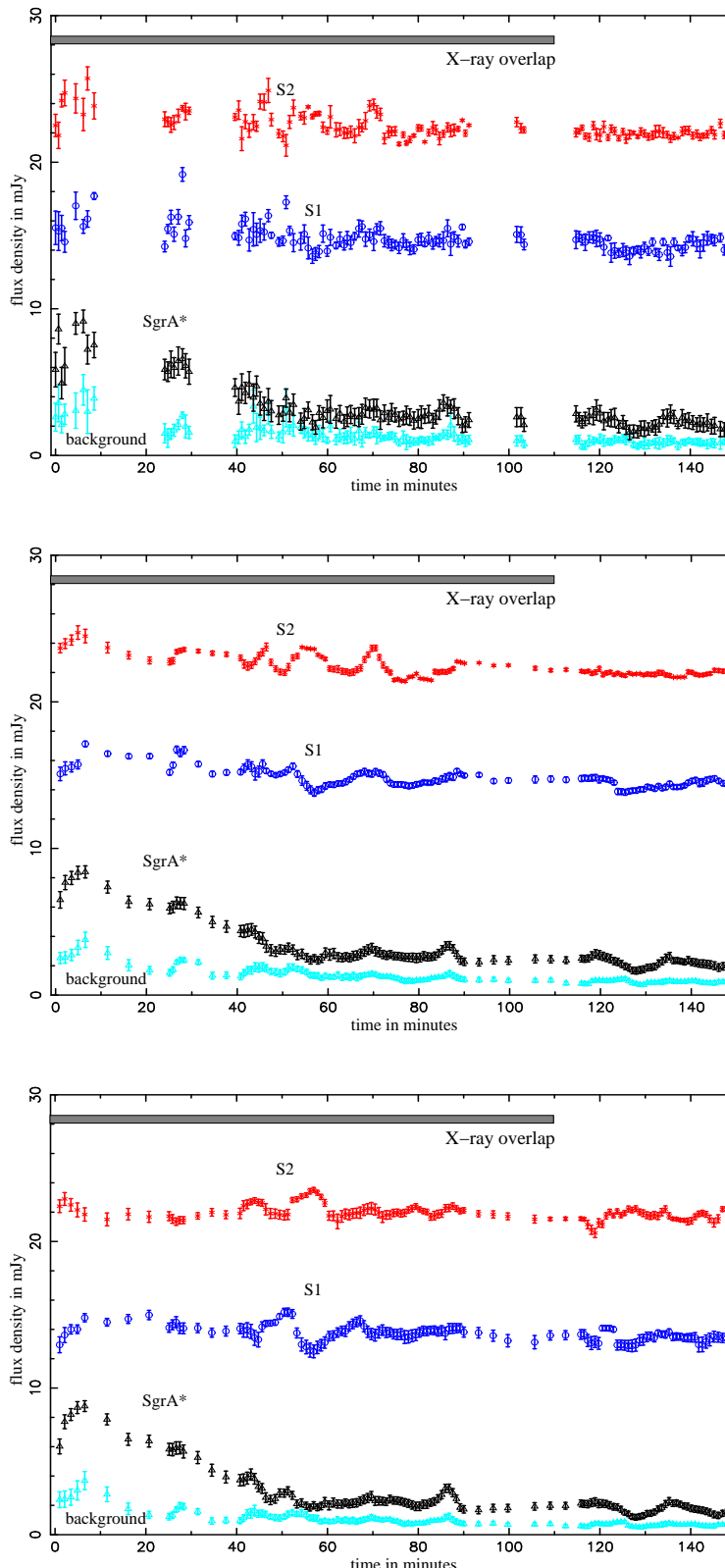


**Fig. 1.** NIR flux variation of Sgr A\* during the coordinated *Chandra*/VLT observations of the Galactic Center. Upper panel: Dereddened NIR flux vs. time of Sgr A\* (black), S1 (green), S2 (red) and of the average of random measurements in a region about  $0.5''$  west of Sgr A\* with no detectable source (blue). Error bars were estimated from aperture photometry with two apertures. The observations started on 19 June 2003 at 23:51:15 (UT). Middle panel: As upper panel, but smoothed with a sliding window, averaging 4 measurements at a time. Lower panel: As middle panel, but corrected for remnant correlated flux variations. The apparent turn down at the beginning of the Sgr A\* light curve (middle and lower panels) affects S1 and

		X-ray	NIR $2.2\mu\text{m}$
zero start time	June 19 UT	23:00 - 23:20	-
zero stop time	June 20 UT	00:15 - 01:05	00:35 - 00:55
FWZP	min	55 - 115	-
FWHM	min	30 - 40	-
decay rate	nJy/min	$0.75^{+1.65}_{-0.45}$	
	mJy/min		$0.12 \pm 0.04$
IQ-state	$\mu\text{Jy}$	$0.015 \pm 0.004$	
flux density	$\text{mJy}$		$1.9 \pm 0.5$
$\alpha_{X/\text{NIR}}$			$1.34 \pm 0.04$
dereddened excess	$\mu\text{Jy}$	$0.039 \pm 0.011$	
flux density	$\text{mJy}$	$3.72 \pm 0.35$	
$\alpha_{X/\text{NIR}}$			$1.29 \pm 0.04$
time lag			$\leq 15 \text{ min}$

**Table 5.** X-ray and NIR Flare and IQ-State Properties. The start and stop times - with an estimated error of 10-15 minutes - refer to those times at which the rising and decaying flanks of the burst deviate from the IQ-state (interim-quiescent) flux density. The spectral indices are defined via  $S_\nu \propto \nu^{-\alpha}$ . The limit on the time lag corresponds to the maximum lag between the decaying flanks of the NIR and X-ray emission of the flare shown in Figures 1 and 3. The burst flux density is given as peak flux density that was measured in excess of the IQ-state flux density. The burst flux was measured for the high S/N measurements taken about 25 min after the beginning of the observations

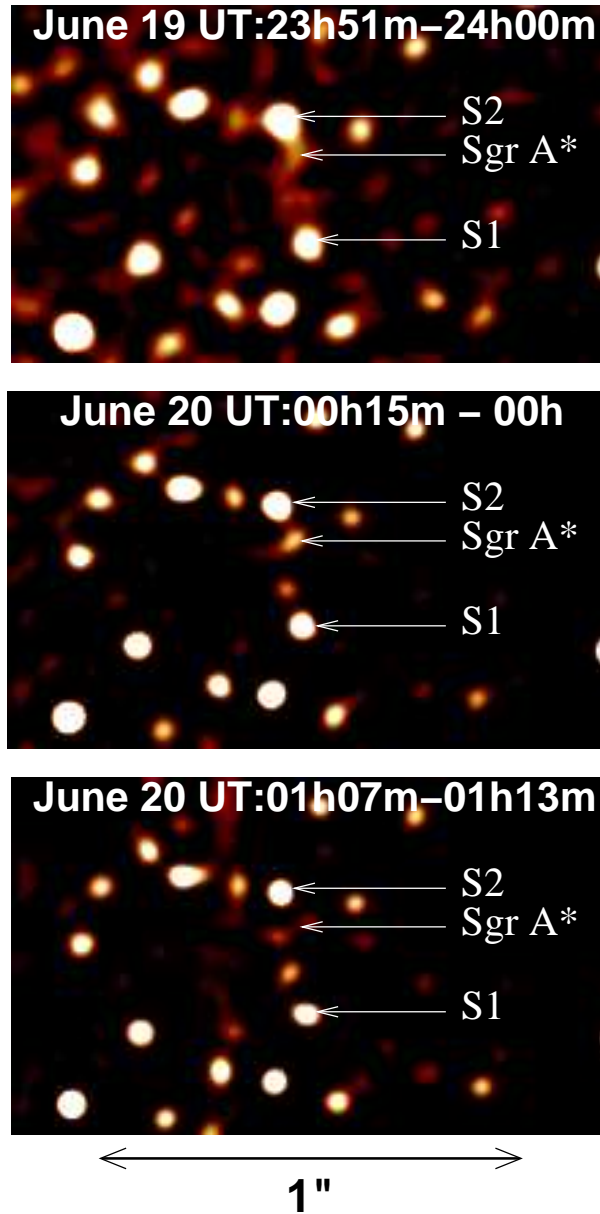


**Fig. 2.** Each panel shows the average of eight Lucy-Richardson deconvolved and beam restored images taken at different intervals of the measurements (see light curves in Figure 1. The UTs of the first image in each series are indicated in the panels. Top: Beginning of the observations. Middle: About 25 min after beginning of the observations. Bottom: Around 80 min after beginning of the observations. One can also see how the image quality improved when comparing the upper and middle/lower panel images. Sgr A\* can be seen as a flaring source in the top and middle panels. The field of view is  $1.43''$  (72 light days) by  $0.85''$  (43 light days).

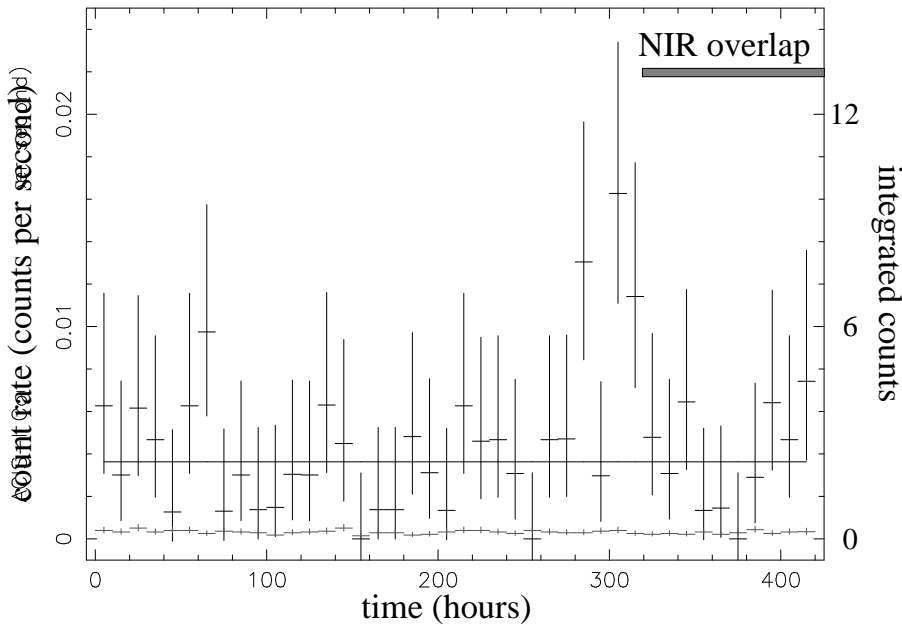


**Fig. 3.** X-ray light curve as observed by *Chandra* in the 1.0'' aperture. The bin interval is 10 minutes. The solid straight line represents the X-ray IQ-state count rate. The background (lower points) was steady throughout the observation. The observations started on 19 June 2003 at 18:51:37 (UT).

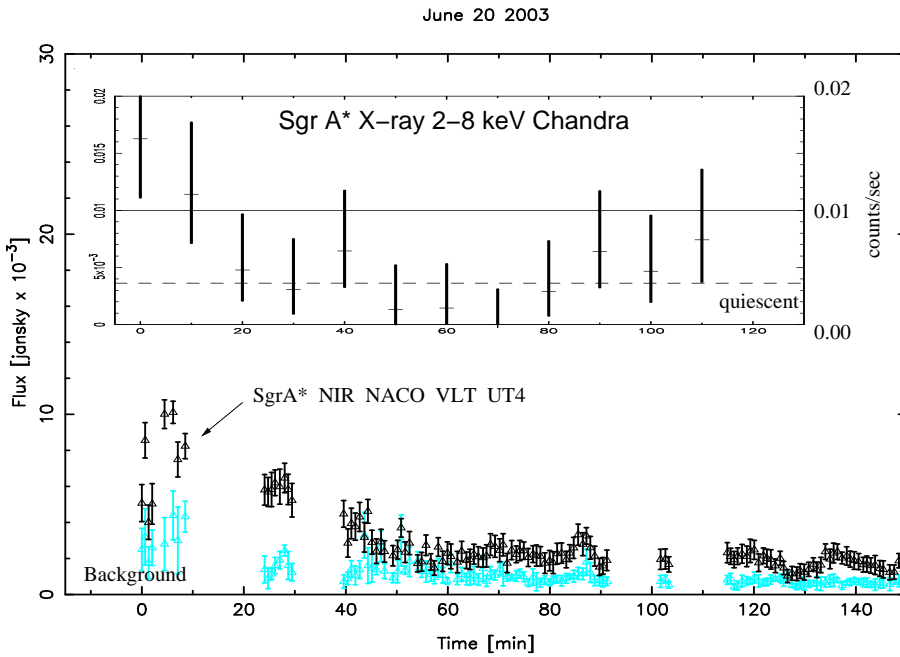


**Fig. 4.** The X-ray and NIR light curves plotted with a common time axis. See text and captions of previous figures. Straight solid lines in the insert box represent the 0.00, 0.01, and 0.02 counts per second levels. The straight dashed line represents the X-ray IQ-state flux density level. The NIR observations started on 19 June 2003 at 23:51:15 (UT); see caption of Figure 1.

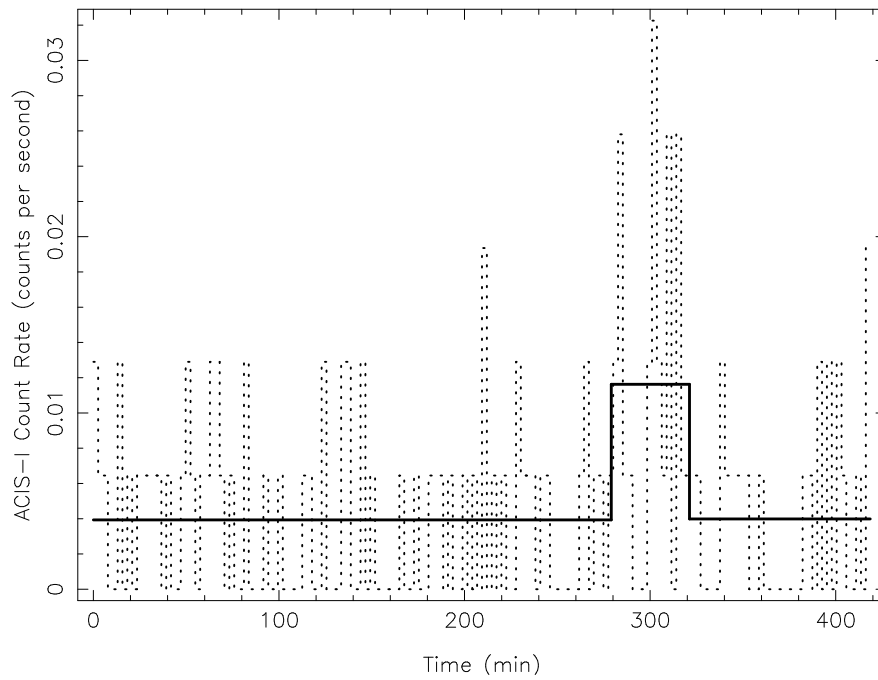


**Fig. 5.** Bayesian blocks representation (solid line) of the X-ray light curve (dashed line) using 157.052 second bins. Two change points detected with 99.927% confidence indicate a flare event around midnight during the interval from 279 to 321 minutes into the observation. The time series starts on 19 June 2003 at 18:51:37 (UT).

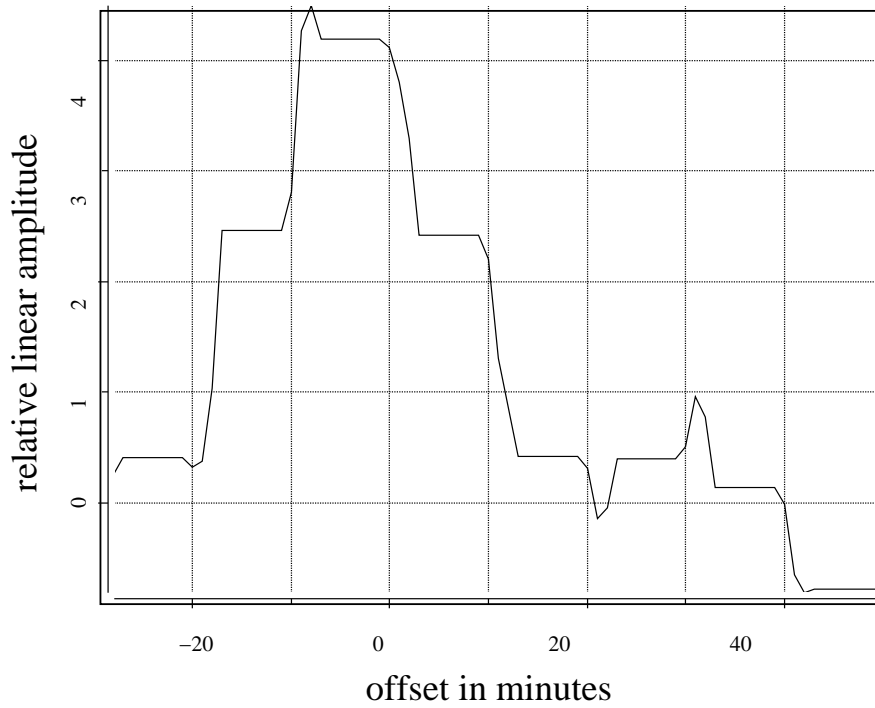


**Fig. 6.** Cross-correlation between the NIR data (40 second bins; 20 seconds intergation time per image) and the X-ray data (10 minute bins). At a  $> 5\sigma$  level both light curves indicate a simultaneous flare event around midnight corresponding to a time delay of less than 15 minutes (see text). Here we cross-correlated only the flare data that overlap in time. The offsets are given in minutes with respect to the beginning of the NIR data at 19 June 23:51:15 (UT). The plot is limited by this start time to the left.